ROYAL SOCIETY OF CHEMISTRY

PAPER

Check for updates

Simultaneous enhancement of thermally activated delayed fluorescence and photoluminescence quantum yield *via* homoconjugation†

Stephanie Montanaro,‡[a] Piotr Pander, [iD] ‡[bc] Jai-Ram Mistry, [iD] [a] Mark R. J. Elsegood, [iD] [a] Simon J. Teat, [iD] [d] Andrew D. Bond, [iD] [e] Iain A. Wright, [iD] *[a] Daniel G. Congrave [iD] *[e] and Marc K. Etherington [iD] *[f]

A critical challenge facing thermally activated delayed fluorescence (TADF) is to facilitate rapid and efficient electronic transitions while ensuring a narrow singlet–triplet energy gap (ΔE_{ST}) in a single luminophore. We present a TADF-active iptycene that clearly demonstrates that homoconjugation can be harnessed as a viable design strategy towards answering this challenge. A homoconjugated analogue of an established quinoxaline-based TADF luminophore has been produced by fusing three of these luminophores together across a shared triptycene core. Homoconjugation was confirmed by electrochemistry, and as a direct consequence of this phenomenon we observed synergistic improvements to photoluminescence quantum yield (Φ_{PL}), radiative rate of singlet decay (k_r^S), delayed fluorescence lifetime (τ_{TADF}), and rate of reverse intersystem crossing (k_{rISC}), all while narrowing the ΔE_{ST}. The enhancement is rationalised with TD-DFT calculations including spin–orbit coupling (SOC). A facile synthesis, the ubiquity of the pyrazine motif in state-of-the-art TADF materials of all colours, and the extent of the overall performance enhancement leads to a great potential for generality.

[a] *Department of Chemistry, Loughborough University, Epinal Way, LE11 3TU, UK.*
 E-mail: i.a.wright@lboro.ac.uk
[b] *Department of Physics, Durham University, South Road, Durham, DH1 3LE, UK*
[c] *Centre for Organic and Nanohybrid Electronics, Silesian University of Technology, Konarskiego 22B, 44-100 Gliwice, Poland*
[d] *Advanced Light Source, Lawrence Berkeley National Laboratory, Cyclotron Road, Berkeley, CA, 94720, USA*
[e] *Yusuf Hamied Department of Chemistry, Cambridge, CB2 1EW, UK.*
 E-mail: dc704@cam.ac.uk
[f] *Department of Mathematics, Physics and Electrical Engineering, Northumbria University, Ellison Place, Newcastle upon Tyne, NE1 8ST, UK.*
 E-mail: marc.k.etherington@northumbria.ac.uk
† Electronic supplementary information (ESI) available. CCDC 2092859–2092861. For ESI and crystallographic data in CIF or other electronic format see DOI: 10.1039/d2tc00460g
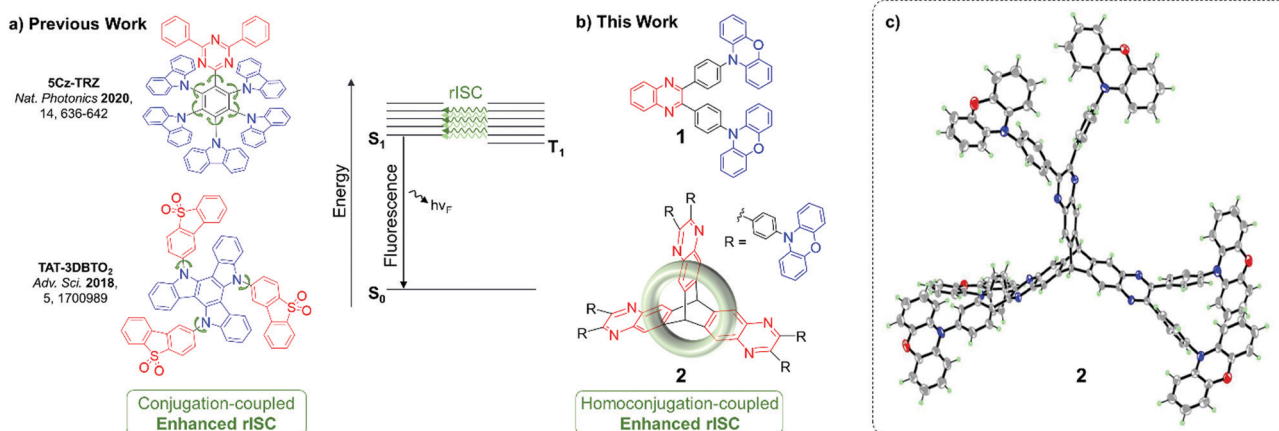‡ These authors have contributed equally to the experimental work.

Introduction

Materials that exhibit thermally activated delayed fluorescence (TADF) are the emergent generation of emitters for organic light-emitting diodes (OLEDs). TADF materials require small singlet–triplet energy gaps (ΔE_{ST}) to enable triplet harvesting *via* reverse intersystem crossing (rISC). rISC is most typically observed in donor–acceptor compounds displaying intramolecular charge transfer (ICT) states which have a large spin–orbit coupling (SOC). The required high SOC is achieved through introducing a manifold of partially delocalised triplet states of both locally-excited (LE) and charge-transfer (CT) character.[1–4]

Structurally, the need for a manifold of states of different characters has translated to ICT molecules built up of numerous weakly coupled chromophores, conjugated through twisted bonds and/or cross conjugation. Prominent examples are **5Cz-TRZ** and **TAT-3DBTO2** reported by Cui, Chen, Adachi, Friend *et al.*[2] and by Bryce, Monkman and co-workers,[5] respectively (Fig. 1a).

To obtain efficient rISC a narrow ΔE_{ST} is necessary. The ΔE_{ST} can be reduced by decreasing the spatial overlap of the electron and hole wavefunctions, which is typically realised by introducing aromatic rings as π-spacers between the donor and acceptor moieties and/or increasing the dihedral angle between said moieties.[1,6,7] Unfortunately, a rapid rISC rate (k_{rISC}) often comes at the expense of a high photoluminescence quantum yield (PLQY, Φ_{PL}) and a fast radiative rate (k_r),[8] as reducing ΔE_{ST} is fundamentally accompanied by a significant reduction in oscillator strength.[5] Hence, molecules capable of combining both a high PLQY and large k_{rISC} are prized in TADF materials development,[2,3,5,9,10] and exploring new molecular design concepts which can synergistically enhance PLQY and k_r alongside k_{rISC} is of vital importance.

Through-space CT (TSCT) can occur in molecules where donor and acceptor moieties are adjacent and proximal,

Fig. 1 (a) Previous and (b) new designs for enhancing TADF through weakly coupled components; (c) X-ray crystal structure of **2**, 7 CHCl$_3$ of crystallisation omitted for clarity.

allowing orbital overlap between the donor and the acceptor through the space between them. This contrasts with through-bond CT (TBCT) observed in traditional organic ICT systems. TSCT has recently gained significant attention towards improving TADF parameters, most notably SOC, as it can support multiple CT states and a large manifold of near-degenerate excited states. Molecules can be designed to show solely TSCT[11–20] or a combination of TBCT and TSCT.[21,22]

Homoconjugation is another non-traditional form of π-electron delocalisation which arises when two conjugated π-systems are separated by a single non-conjugated group, typically an sp^3 carbon atom.[23] It can allow the two π-systems to continue to communicate despite a formal break in conjugation. Triptycene is an archetypal homoconjugated hydrocarbon.[24–29] The unsaturated π-systems of its three phenylene "fins" sit 120° apart, enforced by the two saturated sp^3 bridgehead carbon atoms. Such a rigid conformation forces a trans-annular, through-space overlap between the π-clouds of each phenylene ring (Fig. 1b), resulting in homoconjugated electronic delocalisation which is distinct from conventional through-bond conjugation.[30–33]

Homoconjugation has recently received significant attention in the context of novel luminophores. It has been shown to mediate intramolecular charge transfer between donor and acceptor moieties to introduce efficient TSCT–TADF including spirocyclic[34] and triptycene-based structures.[35–38] A few other TSCT–TADF systems have been synthesised using spirocycles[12,14,18] and triptycene[20] as the scaffolds which link the donor and acceptor moieties. However, in these previous examples the homoconjugated fragments are spectating rather than being actively involved in the TADF process.

A promising phenomenon attributed to homoconjugation in symmetrical iptycenes is an enhancement of π–π* oscillator strength due to cooperative interactions between fins. Experimentally this is observed as a significantly greater than factor of three increase in extinction coefficient (ε) compared with a single fin congener, and is most pronounced when the LUMO is localised over the region of homoconjugation.[39–41] Recently, we

extended this phenomenon to ICT transitions through trimerization of a carbazole-based fluorescent TBCT luminophore which had six *N*-phenylcarbazole moieties linked by a shared, electron-deficient tris(pyrazino)triptycene.[42] The design can be viewed as a core–shell type structure with the HOMO residing over peripheral, electronically isolated donor heterocycles which, upon excitation, push electrons in a TBCT fashion into the LUMO which is localised over the shared homoconjugated triptycene-based acceptor at the centre of the molecule. The design resulted in large enhancements in ICT parameters such as ε, k_r, and PLQY (*i.e.* radiative transitions). Such an approach to harnessing homoconjugation is distinctly different to the previously mentioned existing examples where TSCT takes place between individual donor and acceptor functionalised fins of asymmetric triptycenes or either side of a spirocyclic carbon atom.

To directly address the challenge of sustaining a high PLQY and rapid k_{rISC} we now employ a TADF luminophore in the same fashion to exploit two precedents: (1) the increase of TADF efficiency afforded by weakly coupling numerous chromophores,[2,5] and (2) the enhancement of ICT radiative processes *via* LUMO homoconjugation.[39–42] Simultaneous improvements in both radiative decay and k_{rISC} are realised.

Results and discussion

Design and synthesis

To test our hypothesis the iptycene **2** was synthesised. Three factors led to the selection of this system: (1) the opportunity for comparison with the homologous fin **1**, a known TBCT–TADF emitter,[43] (2) the facile synthesis (Scheme S2.1, ESI†) of quinoxaline-based iptycenes, and (3) the ubiquity of the pyrazine motif in TADF materials.[44–50] The NMR characterisation of the compounds can be found in the ESI† (Fig. S3.1–S3.5). The structure of **2**·7CHCl$_3$ was confirmed by single crystal X-ray diffraction (Fig. 1c and Fig. S4.7, Table S4.3, ESI†). **2** crystallised as a CHCl$_3$ heptasolvate, presumably due to the large internal

This journal is © The Royal Society of Chemistry 2022

J. Mater. Chem. C, 2022, **10**, 6306–6313 | **6307**

free volume of iptycene structures.[51] The interfin angles and distances observed for **2** are essentially identical to those observed for triptycene,[52,53] supporting homoconjugation in **2**. The structure of two, polymorphic, CDCl$_3$ mono-solvates of **1** were also determined using synchrotron radiation (Tables S4.1, S4.2 and Fig. S4.1–S4.6, ESI†). **2** has good thermal stability with a decomposition temperature of 544 °C (T_d corresponding to 5% weight loss) as demonstrated by thermal gravimetric analysis (Fig. S2.1, ESI†). This compares with a T_d of 421 °C reported previously for single fin **1**.[43]

Computational chemistry

1 and **2** were investigated using TD-PBE0/def2-svp (Fig. 2 and Fig. S6.1–S6.34, ESI†).[54] The lowest energy singlet and triplet states for **1** and **2** are predominantly represented by ICT transitions between the phenoxazine donor and quinoxaline acceptor moieties involving the HOMO and LUMO as expected (Fig. S6.1, S6.3, S6.6, S6.9, S6.33 and S6.34, ESI†).[43] For **2** the S$_1$ and S$_2$ states are near-degenerate (Fig. 2a) – a consequence of the localisation of the LUMO/LUMO+1 orbitals of the iptycene core of **2** due to through-space π-system overlap between fins.

Such a MO structure is in agreement with established experimental data for triptycene,[49,55,56] and indicates that homoconjugation should influence the photophysical properties of **2**. Furthermore, IRI-π analysis[57] indicates weak π-interactions between fins, consistent with homoconjugation (Fig. S6.35, ESI†). Narrow ΔE_{ST} values are predicted for **1** and **2** (0.01 and 0.03 eV, respectively). Calculations predict a notably larger oscillator strength (f) for the S$_0$ → S$_1$ transition of **2** than for **1** (f = 0.051 *vs.* 0.003). f is similarly large for the near-degenerate S$_0$ → S$_2$ transition of **2** (f = 0.051). Larger f for the lowest lying singlet states of **2** compared with **1** are promising for enhancements in ε and the radiative rate of singlet decay (k_r^S) (confirmed experimentally below). Furthermore, within <0.4 eV of T$_1$ a manifold of 26 higher energy singlet and triplet states are predicted for the iptycene **2** (Fig. S6.7–S6.32, ESI†), in contrast to only 4 for **1** (Fig. S6.2–S6.5, ESI†). This collection of energetically close excited states (Fig. 2b), comprising numerous CT states spread across the different fins of **2** and a larger number of ^{3}LE states than for **1**, is highly encouraging for accelerated delayed fluorescence in **2**.[2,3,5]

Spin–orbit coupling (SOC) is essential to permit the formally forbidden spin-flip associated with rISC. Hence, the merit of
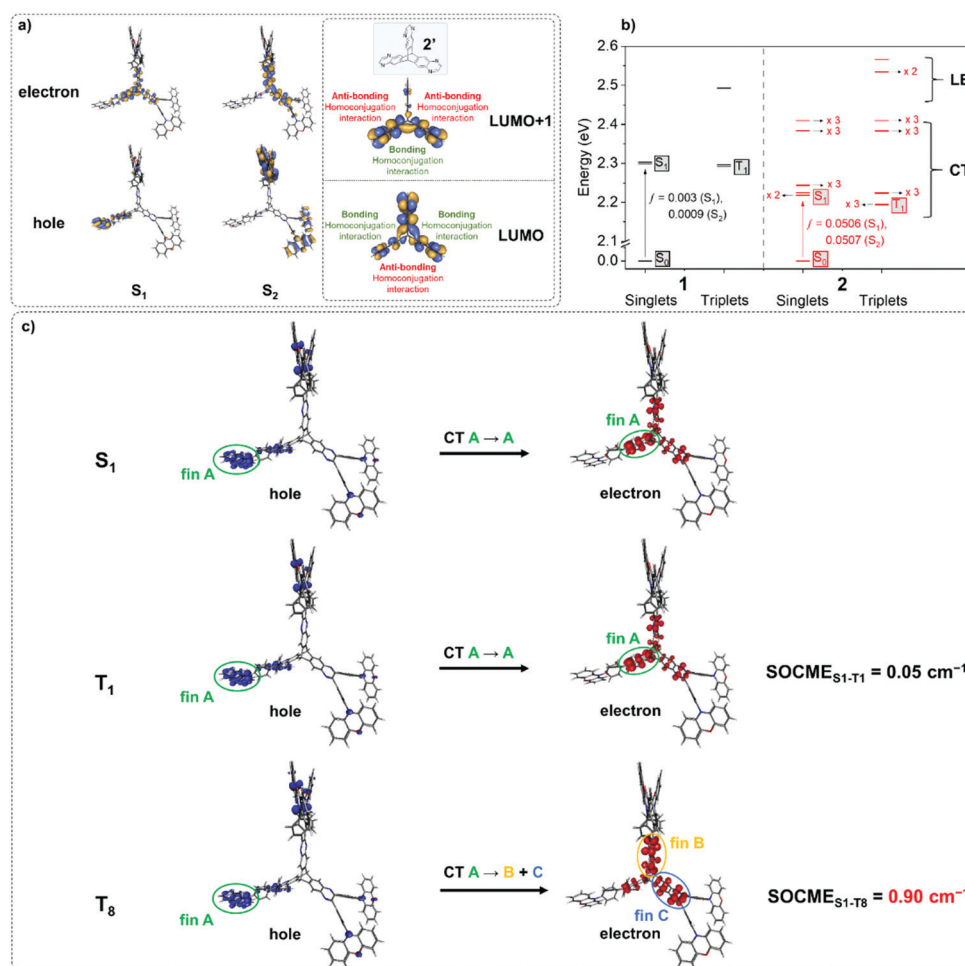

Fig. 2 (a) Natural transition orbitals for S$_1$ and S$_2$ states of **2**. The LUMO and LUMO+1 orbitals of the core **2'** are included to highlight the effect of homoconjugation within the LUMO manifold; (b) Jablonski diagram for **1** and **2**; (c) natural transition orbitals for the S$_1$ and appropriate T states of **2** to highlight spin–orbit coupling.

6308 | *J. Mater. Chem. C*, 2022, **10**, 6306–6313

This journal is © The Royal Society of Chemistry 2022

the manifold of triplet states predicted for **2** was investigated by calculating the spin–orbit coupling matrix elements (SOCMEs) for the ground state optimized structure (TD-PBE0/def2-svp and PySOC script[58]). The relevant states were probed *via* electron–hole analysis with the Multiwfn program to determine their CT or LE character.[59–61] Detailed electron–hole analysis and assignment of excited state character are presented in the ESI† (Section S6 and Table S6.1). Some relevant natural transition orbitals (NTOs) for **2** are shown in Fig. 2c. The fins of **2** in Fig. 2c are denoted A, B and C to aid discussion of the spatial distribution of states. Data for S_1, T_1, and triplet states with SOCME > 0.1 cm^{-1} to S_1 within < 0.4 eV of T_1 are summarized in Table 1 for **1** and **2**.

In agreement with what is intuitive upon visual inspection of the NTOs (Fig. 2a and c), the S_1 state of **2** is assigned as CT in nature. The electron–hole analysis for T_1 is near-identical to that of S_1, meaning both states are the same in configuration (CT) with the same spatial distribution. Hence, as expected from El-Sayed's rule,[62] the calculated S_1–T_1 SOCME is very small (0.05 cm^{-1}), and rISC should be very inefficient between these states. A similar case is observed for the S_1 and T_1 states of **1** (Table 1 and Fig. S6.1, S6.3, ESI†).

It has been accepted that in TADF materials vibronic coupling can facilitate rISC between a CT singlet such as S_1 and upper LE triplet states, for which there should be greater SOC due to a change in excited state configuration.[1–4,10] Indeed, the SOCME values between S_1 and upper LE triplet states (T_3 for **1**; T_{13}, T_{14} and T_{15} for **2**) are of the order of 0.1–0.25 cm^{-1}.

We note for **1** that there is only one LE triplet state (T_3) within 0.4 eV of T_1 with a greater SOCME to S_1 than T_1. This is in stark contrast to what is observed for **2**.

We can explain the more efficient rISC observed experimentally for **2** through the larger presence of states with high SOC. Firstly, **2** has three LE triplets (T_{13}, T_{14} and T_{15}) that exhibit appreciable SOCMEs with S_1. Secondly, due to electronic coupling between the fins of **2**, it is possible to localise CT states across neighbouring fins (Fig. 2c). This is apparent for the T_8 state which is localised differently to S_1. T_8 is a CT state with the

hole predominantly localised on the phenoxazine moieties of fin A, and the electron mainly on the quinoxaline heterocycles of fins B and C with some bridging A contribution. Conversely, for S_1 both the electron and hole are predominantly localised over fin A with some electron density extending onto the quinoxalines of B and C. These distinct differences in the localisation of S_1 and T_8, can translate into a change in orbital angular momentum between the two states, but they crucially retain some spatial overlap over the homoconjugated core of **2**. This enables a large SOCME value of 0.9 cm^{-1} between the CT states S_1 and T_8, which are predicted to be only 0.17 eV apart in energy (Table 1). A significant SOCME is also predicted between S_1 and T_7 (0.29 cm^{-1}), which is a CT state degenerate with T_8 also spread across multiple fins (Table 1 and Fig. S6.18, ESI†).

While the exact rISC mechanism in **2** may be complex, from simply considering the SOCME calculations it is abundantly clear that homoconjugation in **2** can facilitate strong SOC interactions between TADF-relevant states, which are not predicted for the non-homoconjugated single chromophore **1**.

Electrochemistry

1 and **2** display identical first oxidation potentials (E^{ox}) (Fig. 3 and Table S5.1, ESI†), consistent with localisation of the HOMO of **2** on the peripheral phenoxazine donors. Conversely, **2** displays a less negative first reduction potential (E^{red}) than **1**, and hence a more accessible LUMO, which slightly increases its acceptor strength. This can be attributed to the LUMO of **2** being delocalized in a trans-annular fashion over the three quinoxaline rings and provides further evidence of homoconjugation in the LUMO. Additionally, while the first reduction wave for **1** corresponds to what is typically expected for a single electrochemically reversible process, the wave for **2** is clearly a superposition of three electrochemical reductions. This electrochemical behavior supports weak electronic coupling between the multiple fins of **2** through the lower lying unoccupied

Table 1 Summary of computational results

Compound	State	$\Delta E_{S_1–T_n}{}^a$ (eV)	SOCME$_{S_1–T_n}{}^b$ (cm^{-1})	Assignment^c
1	S_1	—	—	CT
	T_1	0.01	0.05	CT
	T_3	−0.19	0.23	LE
2	S_1	—	—	CT A → A
	T_1	0.03	0.05	CT A → A
	T_7	−0.17	0.29	CT B + C → A
	T_8	−0.17	0.90	CT A → B + C
	T_{13}	−0.32	0.11	LE
	T_{14}	−0.32	0.08	LE
	T_{15}	−0.35	0.12	LE

^{a} Calculated energy gap between S_1 and T_n. ^{b} Calculated spin–orbit coupling matrix element between S_1 and T_n. ^{c} A, B and C fin nomenclature is consistent with Fig. 2c; CT = charge transfer, LE = locally excited.
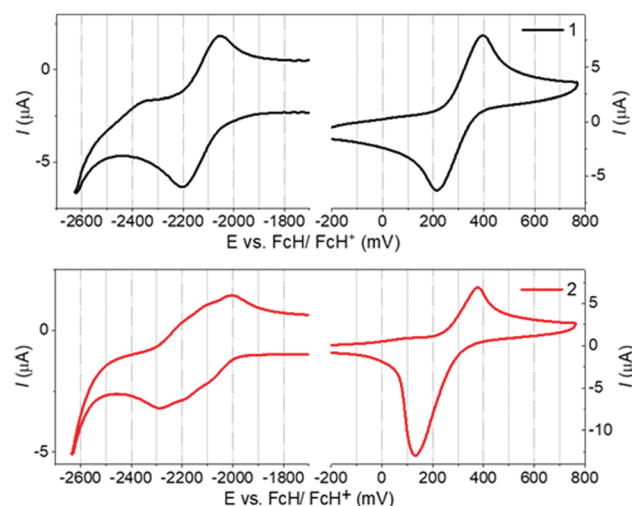

Fig. 3 Cyclic voltammograms for **1** and **2** measured in 0.1 M n-Bu$_4$PF$_6$ in 1,2-dichlorobenzene as the supporting electrolyte. Scan rate = 100 mV s^{-1}.

This journal is © The Royal Society of Chemistry 2022

J. Mater. Chem. C, 2022, **10**, 6306–6313 | **6309**

molecular orbitals, consistent with homoconjugation and the DFT predictions above.

Photophysics

Photophysical measurements (Table 2) in toluene solution (Fig. 4) provide a platform to accurately compare pertinent rates, as the data can be considered intrinsic, with strictly monoexponential decay for both prompt and delayed fluorescence in the absence of any solid-state phenomena. The absorption (and PL) spectrum of **2** is bathochromically shifted compared with that of **1** due to homoconjugation in the LUMO of **2** facilitating a more extended π-structure and thereby a slightly reduced optical band gap. This is consistent with electrochemical and TD-DFT results. The absorption spectra for **1** and **2** consist of intense transitions below *ca.* 350 nm, assigned to π–π* excitations, and lower energy broad ICT transitions ≥400 nm.[63] Similarly, the PL spectra of **1** and **2** are also ascribed to ICT, being broad and featureless and exhibiting positive solvatochromism (Fig. S8.1, ESI†).

As **2** can be considered a molecular trimer of the monomer unit **1**, the maximum ICT absorption extinction coefficient for **2** is expected to be three times that of **1** in the absence of any electronic communication between fins. However, our experimental values, obtained from triplicate measurements on rigorously dried samples, yield a ratio of 3.4 (Table 2) (for **1** $\varepsilon = 3.5 \times 10^3$ M^{-1} cm^{-1} at 398 nm; for **2** $\varepsilon = 12 \times 10^3$ M^{-1} cm^{-1} at 420 nm). An expansion of the ICT region of the UV-vis spectra for **1** and **2** is provided in Fig. S8.2 (ESI†). TD-DFT results indicate that the singlet ICT states of **2** have significant localisation over the homoconjugated iptycene core, while electrochemical measurements also indicate trans-annular orbital overlap between fins. Therefore, the larger than factor of three increase in ICT extinction coefficient for **2** compared with **1** is ascribed to a cooperative effect between the fins of **2** through homoconjugation. Concomitant with this increase, the solution values for Φ_{PL} and k_r^S are considerably enhanced for **2** compared with **1** (**1** − Φ_{PL} = 50%, $k_r^S = 1.8 \times 10^7$ s^{-1}; **2** − Φ_{PL} = 63%, $k_r^S = 2.4 \times 10^7$ s^{-1}). Notably, for **2** the value of k_r^S is increased by a third compared with **1**. Therefore, there is a clear enhancement in the probability of a radiative transition both to and from the ICT state in **2**, crucially observed despite the narrower ΔE_{ST} of **2** compared with **1** (**1** − ΔE_{ST} = 0.26 eV; **2** − ΔE_{ST} = 0.21 eV), as measured in a zeonex host (Table 2 and

Fig. S9.1–S9.9, S10.1, ESI†). The acceleration of radiative transitions in **2** is very likely linked to homoconjugation, in-line with the computational predictions and electrochemical experiments above. We note that electron–hole analysis (Fig. S6.3 and S6.9, ESI†) vaguely suggests that the homoconjugation in **2** leads to an increase in π–π* character of the S_1 state for **2** compared with **1**, which may help explain the improved ε and k_r^S values. Such an enhancement of ICT through homoconjugation has only been noted once previously, in a structure that does not display TADF.[42] Notably, S_1 is also significantly more stabilised than T_1 upon trimerization of compound **1** to **2**, suggesting the iptycene core can be employed to fine-tune the ΔE_{ST} of TADF compounds.

The TADF parameters of **1** and **2** were evaluated in toluene solution (Fig. 4). Both luminophores exhibit a delayed fluorescence (DF) component that spectrally matches the prompt fluorescence (PF) (Fig. 4c and S10.1, ESI†) and contributes similarly to the total Φ_{PL} (**1** − Φ_{DF} = 15%; **2** − Φ_{DF} = 13%). However, the lifetime of the delayed fluorescence (τ_{TADF}) for the iptycene **2**, is nearly five times shorter than that observed for **1** (Fig. 4b), in line with a greater than threefold increase in k_{rISC} (**1** − τ_{TADF} = 27.3 μs, $k_{rISC} = 2.5 \times 10^4$ s^{-1}; **2** − τ_{TADF} = 5.8 μs, $k_{rISC} = 8.7 \times 10^4$ s^{-1}). This is consistent with the dense manifold of energetically close excited states and enhanced SOC in **2** predicted by TD-DFT (Fig. 2), a consequence of intrafin coupling *via* homoconjugation.

To summarise, considered alongside electrochemical and computational studies, the photophysical data obtained for **2** in solution indicate that it is possible to simultaneously amplify the radiative transition probability and k_{rISC} of a TADF luminophore by exploiting homoconjugation. Similar results are obtained in the PVK:PBD blend used for OLED fabrication below *i.e.* a larger PLQY, shorter τ_{TADF}, and faster k_{rISC} for **2** compared with **1** (Fig. S11.1–S11.6, ESI†).

Electroluminescence

Solution-processed OLED devices were fabricated using **1** and **2** as emitters, denoted **Dev 1** and **Dev 2**, respectively. Pertinent data and the device structure are shown in Fig. 5. Additional data are presented in the ESI† (Fig. S12.1 and Table S12.1). The device structure offers low V_{ON} and large current densities, desirable for high device luminance, but also high external quantum efficiency (EQE) due to the presence of an additional

Table 2 The key parameters obtained from the photophysical study of compounds **1** and **2**

	Solvent/matrix	λ_{abs} (nm) [$\varepsilon \times 10^3$ M^{-1} cm^{-1}][a]	λ_{em}[b] (nm)	ΔE_{ST}[c] (eV) [S_1/T_1]	Φ_{PL}[d]	Φ_{PF}	Φ_{DF}	τ_{PF} (ns)	τ_{TADF} (μs)	k_r^{Se} (10^7 s^{-1})	k_{rISC} (10^4 s^{-1})[f]
1	Toluene	332 [26], 398 sh [3.5]	574	—	0.50	0.35	0.15	19.6	27.3	1.8	2.5
	Zeonex	—	504	0.26 [2.74/2.48]	—	—	—	8.9	656	—	—
	PVK:PBD	—	548	0.13 [2.54/2.41]	0.63	0.41	0.22	16.4	26.2	2.5	3.4
2	Toluene	338 [62], 366 [69], 420 sh [12]	583	—	0.61	0.48	0.13	20.5	5.8	2.4	8.7
	Zeonex	—	517	0.21 [2.65/2.44]	—	—	—	12.4	90.1	—	—
	PVK:PBD	—	556	0.06 [2.47/2.41]	0.75	0.49	0.26	24.0	16.7	2.1	6.5

[a] sh = shoulder. [b] Steady state PL maxima. [c] The S_1 energy is taken from delayed fluorescence (and not prompt fluorescence) spectra due to its relevance for the TADF mechanism. [d] Total PLQY in degassed solution or under N_2 in film. [e] Radiative rate of the S_1 state, $k_r^S = \Phi_{PF}/\tau_{PF}$. [f] For calculation details refer to the ESI. All values determined at room temperature except for T_1 energy which is taken from phosphorescence spectra at 80 K.
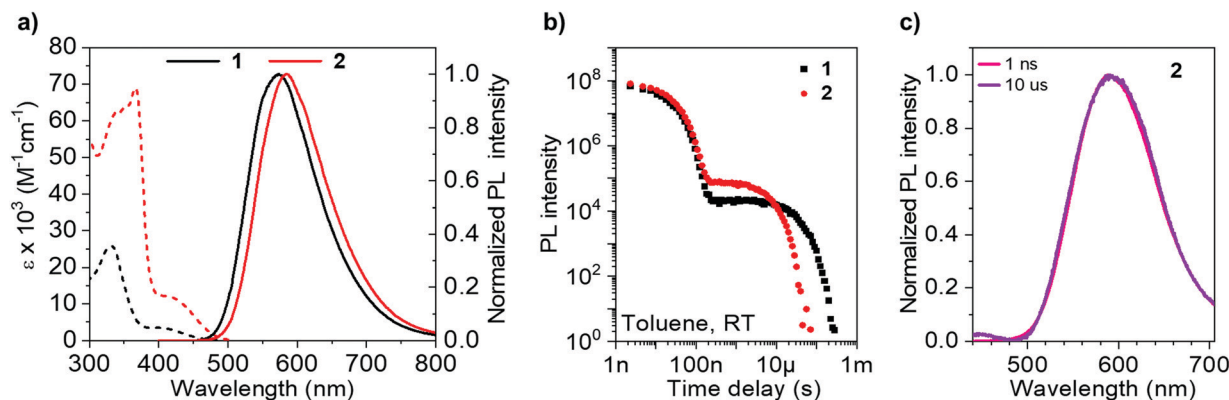
6310 | *J. Mater. Chem. C*, 2022, **10**, 6306–6313

This journal is © The Royal Society of Chemistry 2022

Fig. 4 (a) Extinction coefficient and steady state PL spectra (1×10^{-5} M) of **1** and **2** in toluene; (b) PL decays of **1** and **2** in degassed toluene; (c) prompt and delayed time-resolved spectra for **2** in degassed toluene.
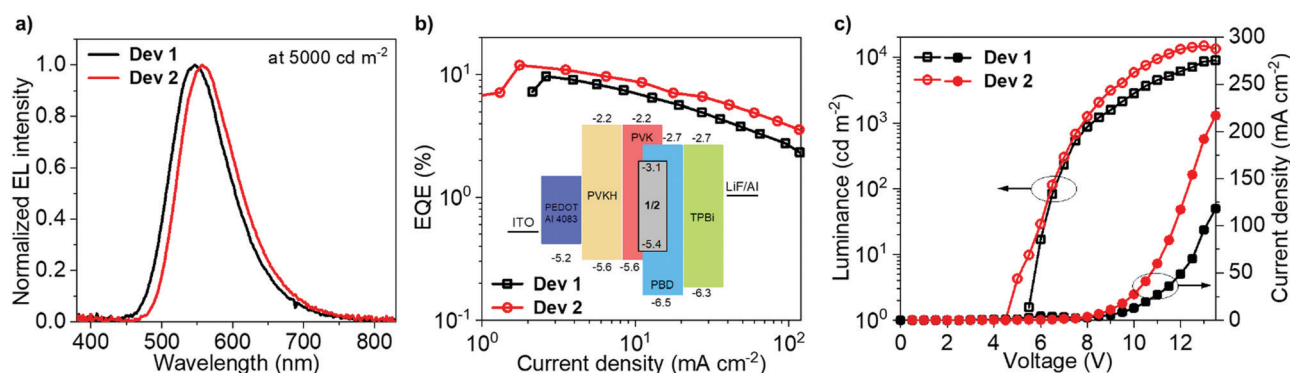

Fig. 5 Electroluminescence characteristics for **Dev 1** and **Dev 2**.

electron blocking PVKH layer.[64] **Dev 1** and **Dev 2** display EQEs reaching maximum values of 9.7% and 11.9%, respectively, in agreement with Φ_{PL} in film, demonstrating a ∼20% increase in efficiency due to homoconjugation. Most crucially, **Dev 2** displays smaller efficiency roll-off than **Dev 1**, thanks to the shorter τ_{TADF} and larger k_{rISC} of **2** in the OLED host (Table 2). The difference in roll-off between **Dev 1** and **Dev 2** is manifested by their diverging characteristics of EQE *vs.* current density in Fig. 5b. The electroluminescence (EL) spectra match the PL in the same host (Table 2). The 11.9% figure is larger than that reported earlier for a similar device structure.[64] While the larger efficiency of **Dev 2** contributes to its greater maximum luminance (**Dev 1** – 8900 cd m^{-2}; **Dev 2** – 14 800 cd m^{-2}), the other significant factor is the higher current density (**Dev 1** – 120 mA cm^{-2}; **Dev 2** – 220 mA cm^{-2}). Both OLEDs show a similar V_{ON} = 5.5–6 V as **1** and **2** have nearly identical HOMO and LUMO energies.

Conclusions

The simultaneous realization of high oscillator strength alongside efficient rISC is essential in the design of next generation TADF materials. For the first time we have proven that it is possible to harness homoconjugation as a viable strategy

towards this objective. By synthesizing a trimer of the known TADF luminophore **1** where the three monomers share an iptycene core, homoconjugation was induced in **2**, which was observed electrochemically. As a direct consequence of the homoconjugation in **2**, simultaneous improvements to PLQY, k_r^S, τ_{TADF}, k_{rISC}, and ΔE_{ST} were achieved, in-line with TD-DFT calculations which predicted a synergistic enhancement of oscillator strength (f) and spin–orbit coupling (SOC). Owing to the facile synthesis of this new system, and the ubiquity of the pyrazine moiety in state-of-the-art TADF materials across the electromagnetic spectrum from the deep blue to the near-infrared (NIR),[44–49] this concept has great promise for generality. NIR TADF emitters in particular are poised to benefit from the enhancement in radiative transitions offered by homoconjugation and will be explored in future work.

Author contributions

S. M. conceptualization, formal analysis, investigation, writing – original draft, writing – review & editing, visualization; P. P. conceptualization, formal analysis, investigation, writing – original draft, writing – review & editing, visualization; J.-R. M. formal analysis (thermal methods), investigation (thermal methods); M. R. J. E. formal analysis (X-ray data sets),

investigation (X-ray crystallography), funding acquisition (ALS beam time), validation (of the structures), visualisation (X-ray structure figures), writing – review & editing; S. J. T. formal analysis (X-ray data sets at the ALS); A. D. B. formal analysis (X-ray data sets), investigation (X-ray Crystallography), validation (of the structures), visualisation (X-ray structure figures). I. A. W. conceptualization, funding acquisition, project administration, supervision, writing – review & editing; D. G. C. conceptualization, project administration, software, visualization, writing – original draft, writing – review & editing; M. K. E. project administration, supervision, writing – review & editing.

Conflicts of interest

There are no conflicts to declare.

Acknowledgements

Notes and references

1 M. K. Etherington, J. Gibson, H. F. Higginbotham, T. J. Penfold and A. P. Monkman, *Nat. Commun.*, 2016, **7**, 13680.
2 L. S. Cui, A. J. Gillett, S. F. Zhang, H. Ye, Y. Liu, X. K. Chen, Z. Sen Lin, E. W. Evans, W. K. Myers, T. K. Ronson, H. Nakanotani, S. Reineke, J. L. Bredas, C. Adachi and R. H. Friend, *Nat. Photonics*, 2020, **14**, 636–642.
3 H. Noda, X. K. Chen, H. Nakanotani, T. Hosokai, M. Miyajima, N. Notsuka, Y. Kashima, J. L. Brédas and C. Adachi, *Nat. Mater.*, 2019, **18**, 1084–1090.
4 J. Gibson, A. P. Monkman and T. J. Penfold, *ChemPhysChem*, 2016, **17**, 2956–2961.
5 P. L. dos Santos, J. S. Ward, D. G. Congrave, A. S. Batsanov, J. Eng, J. E. Stacey, T. J. Penfold, A. P. Monkman and M. R. Bryce, *Adv. Sci.*, 2018, 1700989.
6 H. Uoyama, K. Goushi, K. Shizu, H. Nomura and C. Adachi, *Nature*, 2012, **492**, 234–238.
7 F. B. Dias, K. N. Bourdakos, V. Jankus, K. C. Moss, K. T. Kamtekar, V. Bhalla, J. Santos, M. R. Bryce and A. P. Monkman, *Adv. Mater.*, 2013, **25**, 3707–3714.
8 B. Wex and B. R. Kaafarani, *J. Mater. Chem. C*, 2017, **5**, 8622–8653.
9 X.-K. Chen, Y. Tsuchiya, Y. Ishikawa, C. Zhong, C. Adachi and J.-L. Brédas, *Adv. Mater.*, 2017, **29**, 1702767.
10 X. K. Chen, S. F. Zhang, J. X. Fan and A. M. Ren, *J. Phys. Chem. C*, 2015, **119**, 9728–9733.
11 K. L. Woon, C. L. Yi, K. C. Pan, M. K. Etherington, C. C. Wu, K. T. Wong and A. P. Monkman, *J. Phys. Chem. C*, 2019, **123**, 12400–12410.
12 X. Tang, L. S. Cui, H. C. Li, A. J. Gillett, F. Auras, Y. K. Qu, C. Zhong, S. T. E. Jones, Z. Q. Jiang, R. H. Friend and L. S. Liao, *Nat. Mater.*, 2020, **19**, 1332–1338.
13 H. Tsujimoto, D.-G. Ha, G. Markopoulos, H. S. Chae, M. A. Baldo and T. M. Swager, *J. Am. Chem. Soc.*, 2017, **139**, 4894–4900.
14 S. Y. Yang, Y. K. Wang, C. C. Peng, Z. G. Wu, S. Yuan, Y. J. Yu, H. Li, T. T. Wang, H. C. Li, Y. X. Zheng, Z. Q. Jiang and L. S. Liao, *J. Am. Chem. Soc.*, 2020, **142**, 17756–17765.
15 X. Wang, S. Wang, J. Lv, S. Shao, L. Wang, X. Jing and F. Wang, *Chem. Sci.*, 2019, **10**, 2915–2923.
16 Q. Li, J. Hu, J. Lv, X. Wang, S. Shao, L. Wang, X. Jing and F. Wang, *Angew. Chem., Int. Ed.*, 2020, **59**, 20174–20182.
17 X. L. Chen, J. H. Jia, R. Yu, J. Z. Liao, M. X. Yang and C. Z. Lu, *Angew. Chem., Int. Ed.*, 2017, **56**, 15006–15009.
18 X. Q. Wang, S. Y. Yang, Q. S. Tian, C. Zhong, Y. K. Qu, Y. J. Yu, Z. Q. Jiang and L. S. Liao, *Angew. Chem., Int. Ed.*, 2020, **2**, 5213–5219.
19 H. Miranda-Salinas, Y.-T. Hung, Y.-S. Chen, D. Luo, H.-C. Kao, C.-H. Chang, K.-T. Wong and A. Monkman, *J. Mater. Chem. C*, 2021, **9**, 8819–8833.
20 Y. Wada, H. Nakagawa, S. Matsumoto, Y. Wakisaka and H. Kaji, *Nat. Photonics*, 2020, **14**, 643–649.
21 T. Huang, Q. Wang, S. Xiao, D. Zhang, Y. Zhang, C. Yin, D. Yang, D. Ma, Z. Wang and L. Duan, *Angew. Chem., Int. Ed.*, 2021, **60**, 23771–23776.
22 X. Zheng, R. Huang, C. Zhong, G. Xie, W. Ning, M. Huang, F. Ni, F. B. Dias and C. Yang, *Adv. Sci.*, 2020, **7**, 1–7.
23 IUPAC. Compendium of Chemical Terminology, Gold Book. Compiled by A. D. McNaught and A. Wilkinson, Blackwell Scientific Publications, Oxford, 2nd edn, 1997, ISBN 0-9678550-9-8, DOI: 10.1351/goldbook.
24 P. D. Bartlett, M. J. Ryan and S. G. Cohen, *J. Am. Chem. Soc.*, 1942, **64**, 2649–2653.
25 K. Baumgärtner, M. Hoffmann, F. Rominger, S. M. Elbert, A. Dreuw and M. Mastalerz, *J. Org. Chem.*, 2020, **85**, 15256–15272.
26 N. Harada, H. Uda, K. Nakasuji and I. Murata, *J. Chem. Soc., Perkin Trans. 2*, 1989, 1449–1453.
27 T. Nakazawa and I. Murata, *J. Am. Chem. Soc.*, 1977, **99**, 1996–1997.
28 N. Harada, Y. Tamai, Y. Takuma and H. Uda, *J. Am. Chem. Soc.*, 1980, **102**, 501–506.
29 H.-D. Martin and B. Mayer, *Angew. Chem., Int. Ed. Engl.*, 1983, **22**, 283–314.

6312 | *J. Mater. Chem. C*, 2022, **10**, 6306–6313

This journal is © The Royal Society of Chemistry 2022

30 J. Li, P. Shen, Z. Zhao and B. Z. Tang, *CCS Chem.*, 2019, **1**, 181–196.

31 L. T. Scott, *Pure Appl. Chem.*, 1986, **58**, 105–110.

32 A. Braendle, A. Perevedentsev, N. J. Cheetham, P. N. Stavrinou, J. A. Schachner, N. C. Mösch-Zanetti, M. Niederberger and W. R. Caseri, *J. Polym. Sci., Part B: Polym. Phys.*, 2017, **55**, 707–720.

33 L. T. Scott and M. M. Hashemi, *Tetrahedron*, 1986, **42**, 1823–1830.

34 Y. K. Wang, C. C. Huang, H. Ye, C. Zhong, A. Khan, S. Y. Yang, M. K. Fung, Z. Q. Jiang, C. Adachi and L. S. Liao, *Adv. Opt. Mater.*, 2020, **8**, 1–7.

35 K. Kawasumi, T. Wu, T. Zhu, H. S. Chae, T. Van Voorhis, M. A. Baldo and T. M. Swager, *J. Am. Chem. Soc.*, 2015, **137**, 11908–11911.

36 Y. Gao, T. Su, Y. Wu, Y. Geng, M. Zhang and Z. M. Su, *Chem. Phys. Lett.*, 2016, **666**, 7–12.

37 C. C. A. Voll, J. U. Engelhart, M. Einzinger, M. A. Baldo and T. M. Swager, *Eur. J. Org. Chem.*, 2017, 4846–4851.

38 P. Lei, S. Zhang, N. Zhang, X. Yin, N. Wang and P. Chen, *ACS Omega*, 2020, **5**, 28606–28614.

39 L. Lv, W. Sun, Z. Jia, G. Zhang, F. Wang, Z. Tan and L. Zhang, *Mater. Chem. Front.*, 2020, **4**, 3539–3545.

40 T. Kodama, Y. Hirao, T. Nishiuchi and T. Kubo, *ChemPlusChem*, 2017, **82**, 1006–1009.

41 T. Kodama, S. Miyazaki and T. Kubo, *ChemPlusChem*, 2019, **84**, 599–602.

42 S. Montanaro, D. G. Congrave, M. K. Etherington and I. A. Wright, *J. Mater. Chem. C*, 2019, **7**, 12886–12890.

43 L. Yu, Z. Wu, C. Zhong, G. Xie, Z. Zhu, D. Ma and C. Yang, *Adv. Opt. Mater.*, 2017, **5**, 1700588.

44 J. Liu, K. Zhou, D. Wang, C. Deng, K. Duan, Q. Ai and Q. Zhang, *Front. Chem.*, 2019, **7**, 312.

45 T. Huang, D. Liu, J. Jiang and W. Jiang, *Chem. – Eur. J.*, 2019, **25**, 10926–10937.

46 P. Rajamalli, D. Chen, S. M. Suresh, Y. Tsuchiya, C. Adachi and E. Zysman-colman, *J. Subst. Abuse Treat.*, 1996, **13**, 287–288.

47 K. Zhang, F. Yang, Y. Zhang, Y. Ma, J. Fan, J. Fan, C.-K. Wang and L. Lin, *J. Phys. Chem. Lett.*, 2021, **12**, 1893–1903.

48 U. Balijapalli, R. Nagata, N. Yamada, H. Nakanotani, M. Tanaka, A. D'Aléo, V. Placide, M. Mamada, Y. Tsuchiya and C. Adachi, *Angew. Chem., Int. Ed.*, 2021, **60**, 8477–8482.

49 P. Meti, H. H. Park and Y. D. Gong, *J. Mater. Chem. C*, 2020, **8**, 352–379.

50 L. Salah, M. K. Etherington, A. Shuaib, A. Danos, A. A. Nazeer, B. Ghazal, A. Prlj, A. T. Turley, A. Mallick, P. R. McGonigal, B. F. E. Curchod, A. P. Monkman and S. Makhseed, *J. Mater. Chem. C*, 2021, **9**, 189–198.

51 T. M. Long and T. M. Swager, *Adv. Mater.*, 2001, 601–604.

52 R. G. Hazell, G. S. Pawley and C. E. Lund Petersen, *J. Cryst. Mol. Struct.*, 1971, **1**, 319–324.

53 W. F. Sanjuan-Szklarz, A. A. Hoser, M. Gutmann, A. Ø. Madsen and K. Woźniak, *IUCrJ*, 2016, **3**, 61–70.

54 S. Grimme, J. Antony, S. Ehrlich and H. Krieg, *J. Chem. Phys.*, 2010, **132**, 154104.

55 M. V. Ivanov, S. A. Reid and R. Rathore, *J. Phys. Chem. Lett.*, 2018, **9**, 3978–3986.

56 M. R. Talipov, T. S. Navale and R. Rathore, *Angew. Chem., Int. Ed.*, 2015, **54**, 14468–14472.

57 T. Lu and Q. Chen, *Chem. Methods*, 2021, **1**, 231–239.

58 X. Gao, S. Bai, D. Fazzi, T. Niehaus, M. Barbatti and W. Thiel, *J. Chem. Theory Comput.*, 2017, **13**, 515–524.

59 T. Lu and F. Chen, *J. Comput. Chem.*, 2011, **33**, 580–592.

60 W. Zeng, T. Zhou, W. Ning, C. Zhong, J. He, S. Gong, G. Xie and C. Yang, *Adv. Mater.*, 2019, 1901404.

61 W. Zhuang, S. Wang, Q. Tao, W. Ma, M. Berggren, S. Fabiano, W. Zhu and E. Wang, *Macromolecules*, 2021, **54**, 970–980.

62 M. A. El-Sayed, *J. Chem. Phys.*, 1963, **38**, 2834–2838.

63 P. Data, P. Pander, M. Okazaki, Y. Takeda, S. Minakata and A. P. Monkman, *Angew. Chem., Int. Ed.*, 2016, **55**, 5739–5744.

64 R. Pashazadeh, P. Pander, A. Lazauskas, F. B. Dias and J. V. Grazulevicius, *J. Phys. Chem. Lett.*, 2018, **9**, 1172–1177.

This journal is © The Royal Society of Chemistry 2022

J. Mater. Chem. C, 2022, **10**, 6306–6313 | **6313**